SUPPLEMENTARY MATERIAL

SUPPLEMENTARY FIGURES

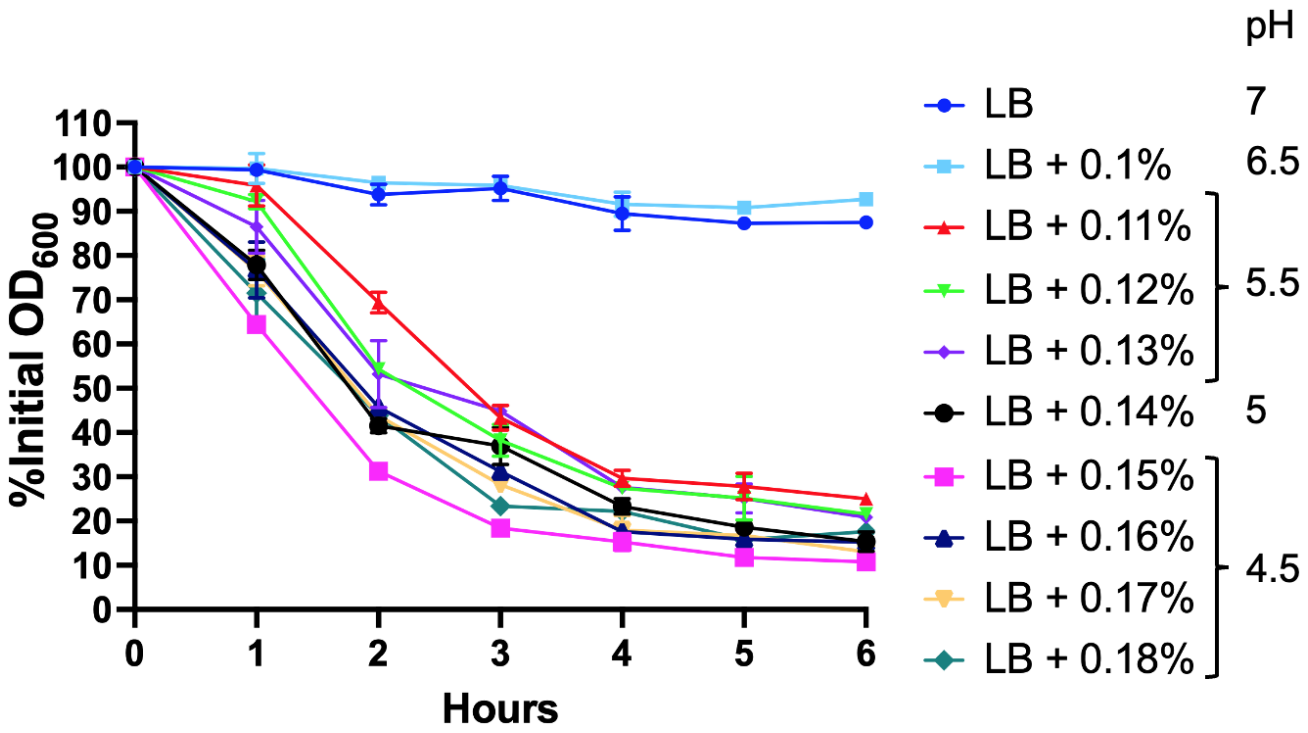

Supplementary Figure S1. Kinetics of YfaL-mediated auto-aggregation correlates with increased sugar concentration and drop of pH. The figure displays aggregation curves monitored in tube. Bacteria were grown in the presence of fructose at different concentrations and pH was measured for each culture at the end of the growth. Results are expressed as a percentage of the OD measured at the top of the tube at T0, time at which the cultures were homogenized. For each strain a measurement is taken at the exact same position in the tube throughout time. A 100 % OD measurement corresponds to the absence of aggregation, and a decrease in % OD indicates aggregate formation. Plotted data represent the mean ± standard deviation of 2 biological replicates (n=2, each replicate is the mean of 2 technical replicates).

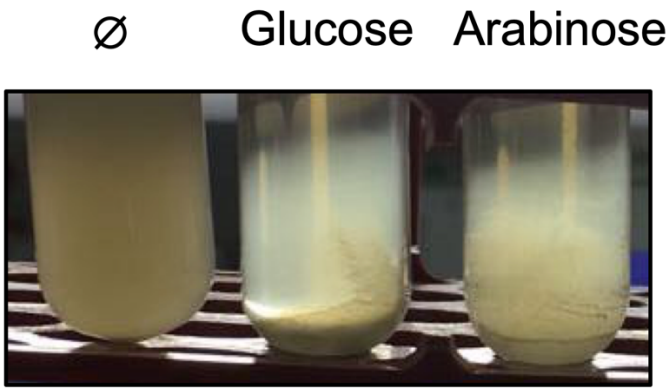

Supplementary Figure S2. YfaL-mediated auto-aggregation still depends on sugar addition when considering a strain deleted for other *E. coli* main cell-surface appendages. Macroscopic observation of aggregate formation by the strain PcL*yfaL* expressing *yfaL* but deleted for the main other cell surface appendages expressed in *E. coli*: Ag43, type 1 fimbriae, curli and flagella (strain PcL*yfaL*_Δ*ag43*_Δ*fim*_Δ*csgA*_Δ*fli*). Tubes correspond to experiments performed in the absence of sugar in the growth medium, and in the presence of glucose or arabinose (specified).

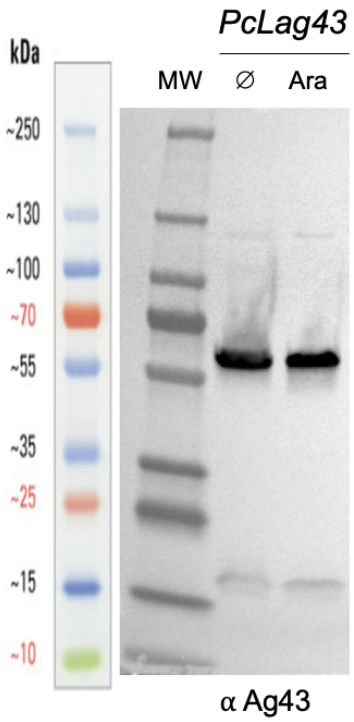

Supplementary Figure S3. Constitutive PcL-mediated production of Ag43 is not impacted by the presence of sugar. Western blot of whole cell extracts from PcL*ag43* strain grown in LB or LB ara, using a primary rabbit antibody directed against the passenger domain of Ag43 and a secondary antibody HRP-linked anti-rabbit. Ara=arabinose. Unlike for YfaL, neither the quantity nor the pattern of migration of Ag43 is affected by the presence of arabinose in the growth medium and therewith by a sugar-induced medium acidification.

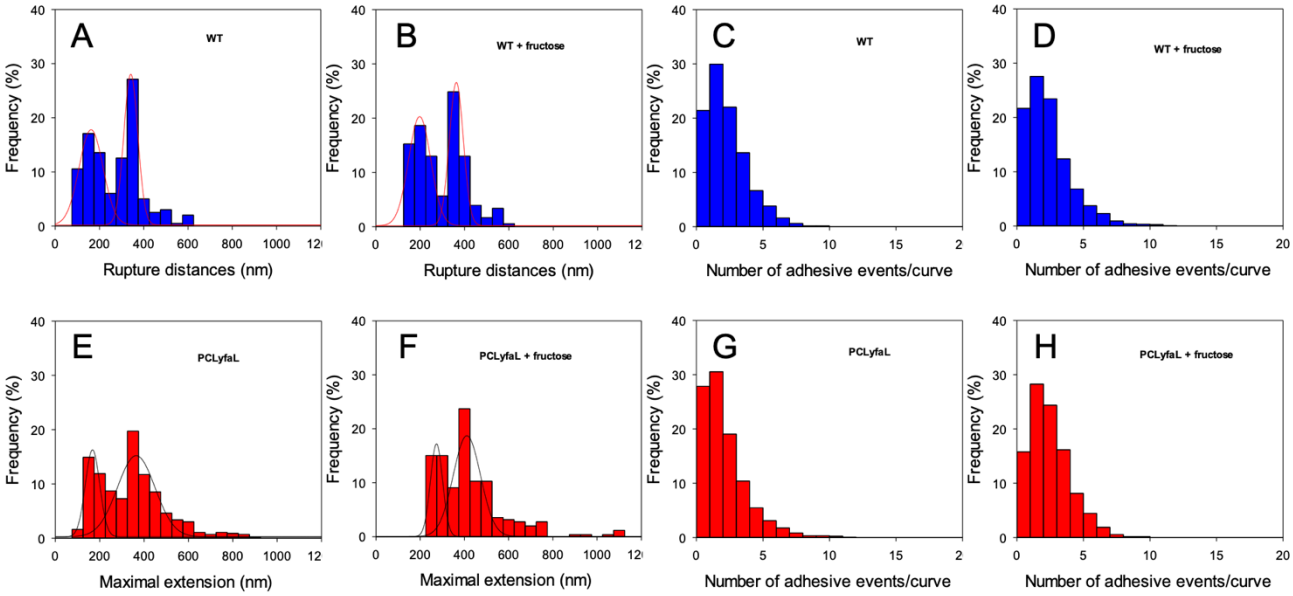

Supplementary Figure S4: Rupture distances and number of adhesive events on *E. coli* WT (blue) and *E. coli* PcL*yfaL* (red) strains grown in LB with or without 0.3% fructose. Statistical distribution of maximal distance measured on *E. coli* WT (blue) and *E. coli* PcL*yfa*L (red) strains grown in LB with or without 0.3% fructose (A, B, E, and F). The rupture distances were evaluated from the analysis of the last rupture event of the cell-to-tip retraction force curve. Statistical distribution of the number of adhesive events per force curve measured on *E. coli* WT (blue) and *E. coli* PcL*yfaL* (red) strains grown in LB with or without 0.3% fructose (C, D, G, and H). The number of adhesive events per force curve according to cell growth conditions were calculated from the analysis of all rupture or adhesive events. These data were obtained from experiments performed on 10 individual bacterial cells at least.

Supporting information text:

The absence of clear connections between the bimodal distribution of rupture events and the YfaL structure are further supported by the distributions of the number of adhesive events per force curve that we report below for the 4 conditions of interest (absence/presence of sugar, WT/PcL*yfaL* cells). With these graphs, we observe the absence of any clear trend in the way the distributions are modified from WT to PcL*yfaL* cells with or without sugar: all distributions look rather similar within experimental error. However, one can emphasize that the number of rupture events/per curve increases significantly only for the PcL*yfaL* strain in presence of sugar.

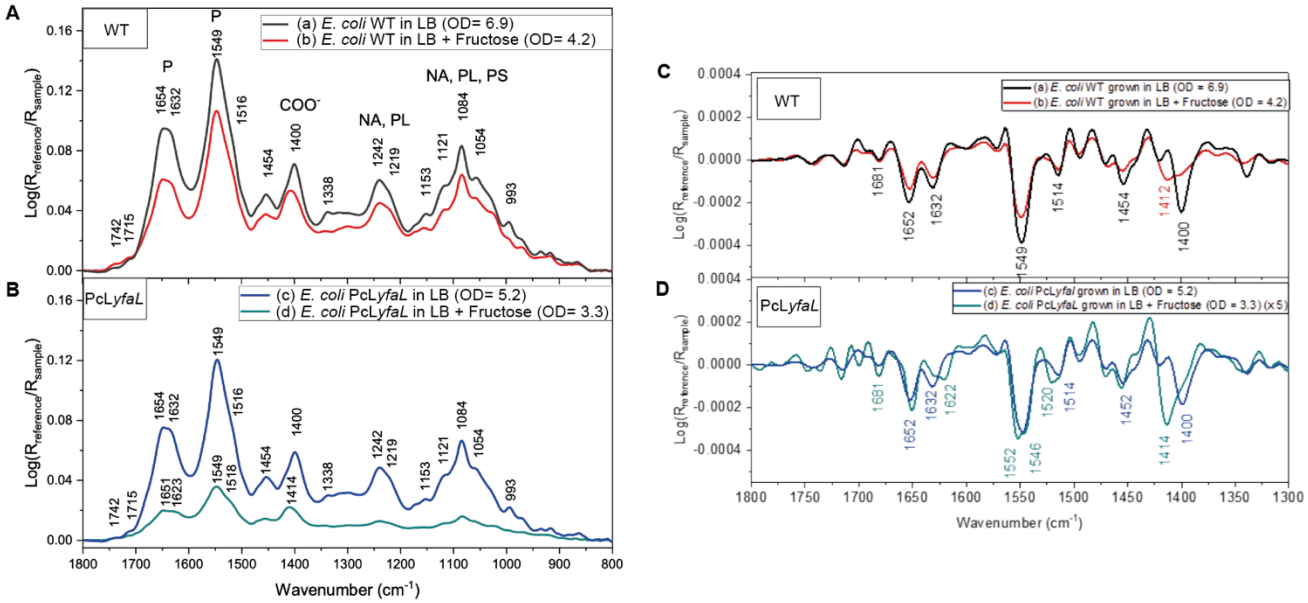

Supplementary Figure S5: Infrared spectroscopy allows detecting the overproduction of PcL*yfaL* and acetate in *E. coli*. (A, B) Infrared spectra in ATR mode of the *E. coli* suspensions grown in LB (Aa) and (Bc) or in LB supplemented with 0.3% fructose (Ab) and (Bd) after 4 hours of deposition on the diamond ATR crystal. (A) *E. coli* wild type (WT), (B) *E. coli* PcL*yfaL*. Abbreviations: P, proteins; NA, nucleic acids; PL, phospholipids, PS, polysaccharides. (C) and (D) Second derivative spectra in the region 1800-1300 cm^{-1} of the spectra presented in (A) and (B), respectively. The second derivative spectrum of *E. coli* PcL*yfal* was multiplied by 5 to get a direct comparison between conditions. Integrated intensities for proteins (P), nucleic acids and phospholipids (NA+PL), and nucleic acids, phospholipids and polysaccharides NA+PL+PS) were calculated from 1596-1484, 1277-1186, and 1199-950 cm^{-1}, respectively.

Supporting information text:

Figure S5 shows the infrared spectra of WT and PcL*yfaL* strains grown overnight in LB with or without 0.3% fructose. The spectroscopic fingerprints make it possible to identify the biochemical components of bacterial cells, i.e. proteins (P), nucleic acids (NA), phospholipids (PL) and polysaccharides (PS) (cf. assigned spectra in **Figure S5A-B**). The spectra highlight slight differences. Strains grown in LB showed the COO^- stretching band at 1400 cm^{-1} assigned to the symmetric stretching of COO^- from proteins. The maximum of this band is shifted to 1410 cm^{-1} for both strains grown in LB supplemented with 0.3% fructose. The second derivative spectra in the region 1800-1300 cm^{-1} (**Figure S5C-D**) allow to resolve the bands at 1681, 1652, 1632, 1549, 1514 and 1400 cm^{-1} for bacteria grown in LB. An additional small band is detected at 1412 cm^{-1} for *E. coli* WT grown in LB supplemented with fructose. For *E. coli* PcL*yfaL* grown in LB supplemented with fructose, bands at 1414 and 1552 cm^{-1} are resolved. In agreement with medium acidification in the presence of fructose, these bands are assigned to COO^- stretching bands from acetate [1] basically because *E. coli* can produce acetate/acetic acid from fructose by fermentation [2]. In the amide bands region (1700-1500 cm^{-1}), two additional bands occur at 1622 and 1520 cm^{-1} for *E. coli* PcL*yfaL* grown in LB supplemented with

fructose (**Figure S5D)**. They are assigned to amide I and II bands for β-sheets secondary structures of proteins [3], therefore indicating that the signature of YfaL is detected in *E. coli* PcL*yfaL* only when fructose is present. The fitting of the broad amide I band into individual bands reveals that the percentage of β-sheets increases from 38% to 45% for the PcL*yfaL* strain grown in LB vs LB supplemented with 0.3% fructose. The calculated integrated areas ratios of P/{NA+PL} [4, 5] for both strains are on average 2.42 and 2.14 in LB and in LB supplemented with 0.3% fructose, respectively. As bacteria are roughly 50% protein, and as their content does not usually vary dramatically under different growth conditions, these values show the higher content of nucleic acids in *E. coli* grown in LB supplemented with 0.3% fructose, and they suggest a higher general metabolic activity in LB supplemented with fructose. In addition, the calculated integrated areas ratios {NA+PL}/{NA+PL+PS} are 0.39 in LB, and 0.44 in LB supplemented with 0.3% fructose for *E. coli* PcL*yfaL*. This result suggests that the production of extracellular polysaccharidic derivatives (called PS above) is lower in the medium supplemented with fructose for *E. coli* PcL*yfaL*.

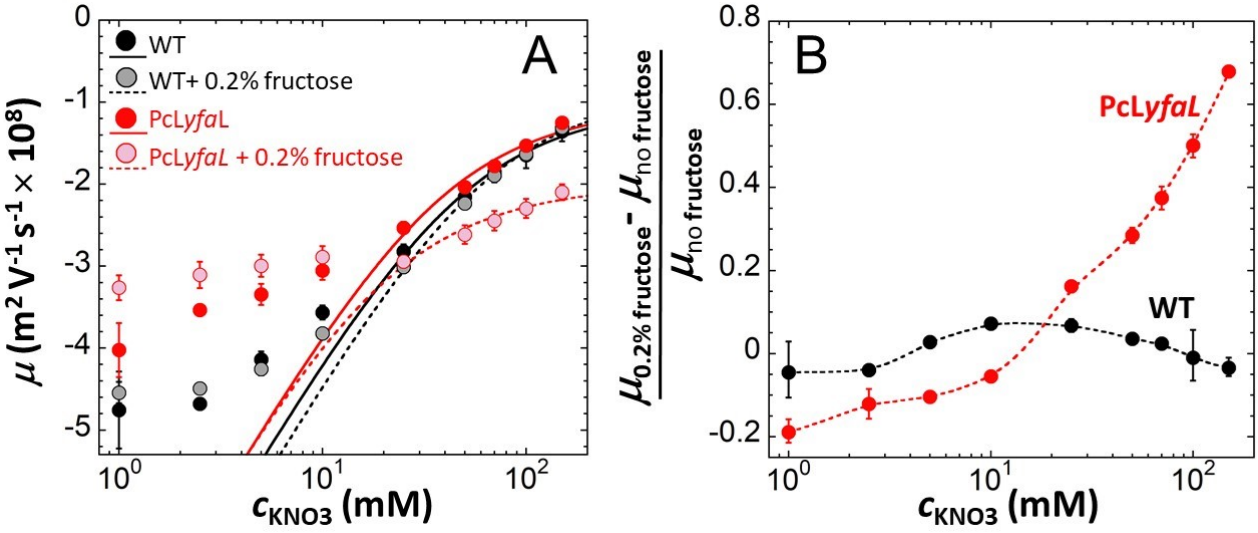

Supplementary Figure S6. **Cell electrokinetics evidence minor effects of post-growth pH modification on cell surface electrostatic and flow-permeability properties as compared to effects of sugar during cell growth.** Dependence of the electrophoretic mobility, μ, of WT and PcL*yfaL* on KNO_3 electrolyte concentration, c_{KNO3}, at pH 5.7 after growth in the presence or absence of 0.2% fructose (indicated). In **(A)**, dotted lines are fits of electrophoretic data using Ohshima equations (1)-(4) valid at sufficiently large c_{KNO3} (see details in Materials section). In **(B)**, symbols represent relative changes in the electrophoretic mobility of WT and PcL*yfaL* grown in the presence of fructose as compared to the situation where fructose is absent from the growth medium. Dotted lines in **(B)** are guides to the eye. Each data point in this figure corresponds to a triplicate measurement (n=3).

Supporting information text:

Supplementary Figure S6 reports electrophoretic measurements performed for PcL*yfaL* and WT strains under the scenarios tested in **Figures 5A,B** (i.e. presence/absence of fructose, variation in KNO_3 concentration)**,** albeit in KNO_3 solution with pH value 5.7 and with a slightly lower fructose content (when present) in growth medium (0.2% instead of 0.3% in **Figures 5A,B**). Briefly, the electrophoretic profiles collected under such conditions qualitatively conform to those obtained at lower pH and higher fructose concentration. Namely, unlike for WT, the addition of fructose leads for *PcLyfaL* to a noticeable 2-fold reduction of the charge density $|\rho_o|$ and to a 2-fold increase of the flow penetration length $1/\lambda_o$ within the cell surface layer (**Supplementary Table S4**)**.** Remarkably, these changes of $|\rho_o|$ and $1/\lambda_o$ are significantly less marked than those estimated at pH 4.6 and 0.3% fructose concentration. This is a consequence of the less pronounced flattening of the μ versus c_{KNO3} curves for PcL*yfaL* when switching from fructose-free growth medium to a medium containing 0.2% fructose (**Supplementary Figure S6A)**, this flattening being weaker than that commented in **Figure 5A**. In contrast to **Figure 5A**, we do not observe in **Supplementary Figure S6A** any significant differences between the μ versus c_{KNO3} profiles measured for WT in the presence and absence of fructose at c_{KNO3}<20 mM. Given that the charge and flow-permeation properties estimated from SSE formalism for WT are of the same order of magnitude for these two conditions (**Supplementary Table S4**) at both pH 5.7 and 4.6, we anticipate that difference in μ at c_{KNO3}<20 mM for the WT originates from enhanced heterogeneity of the WT/solution interface, recalling that this heterogeneity is best revealed at low salt concentration [6]. As a final comment, data collected in **Supplementary Table S4** for WT in the absence of fructose confirms the expected (slight to moderate) decrease of $|\rho_o|$ with

decreasing pH due to weaker dissociation of hydroxyl and carboxyl surface groups [7], a finding that also holds when decreasing solution pH from 5.7 to 4.6 for WT grown in the presence of 0.2%-0.3% fructose and for PcL*yfaL* grown in the absence of fructose. The $1/\lambda_o$ values relative to these different conditions hardly vary with changing (post-growth) pH, meaning that pH predominantly affects the only electric double layer charging at the cell/solution interface within the configurations (absence/presence of sugar + absence of YfaL) and (absence of sugar + presence of YfaL). Finally, we observe that the electrophoretic profiles of PcL*yfaL* and WT at pH 5.7 and 4.6 (**Figure 5A**) grown in the absence of fructose are similar at c_{KNO3}>30-40 mM and that they significantly differ at lower c_{KNO3}. This result is qualitatively in line with the electrokinetic data and conclusions reported by Francius et al. for *E. coli* cells differing in terms of expressed surface appendages [8], i.e. a better discrimination of surface phenotypes of bacteria is achieved by electrophoresis at sufficiently low electrolyte concentrations.

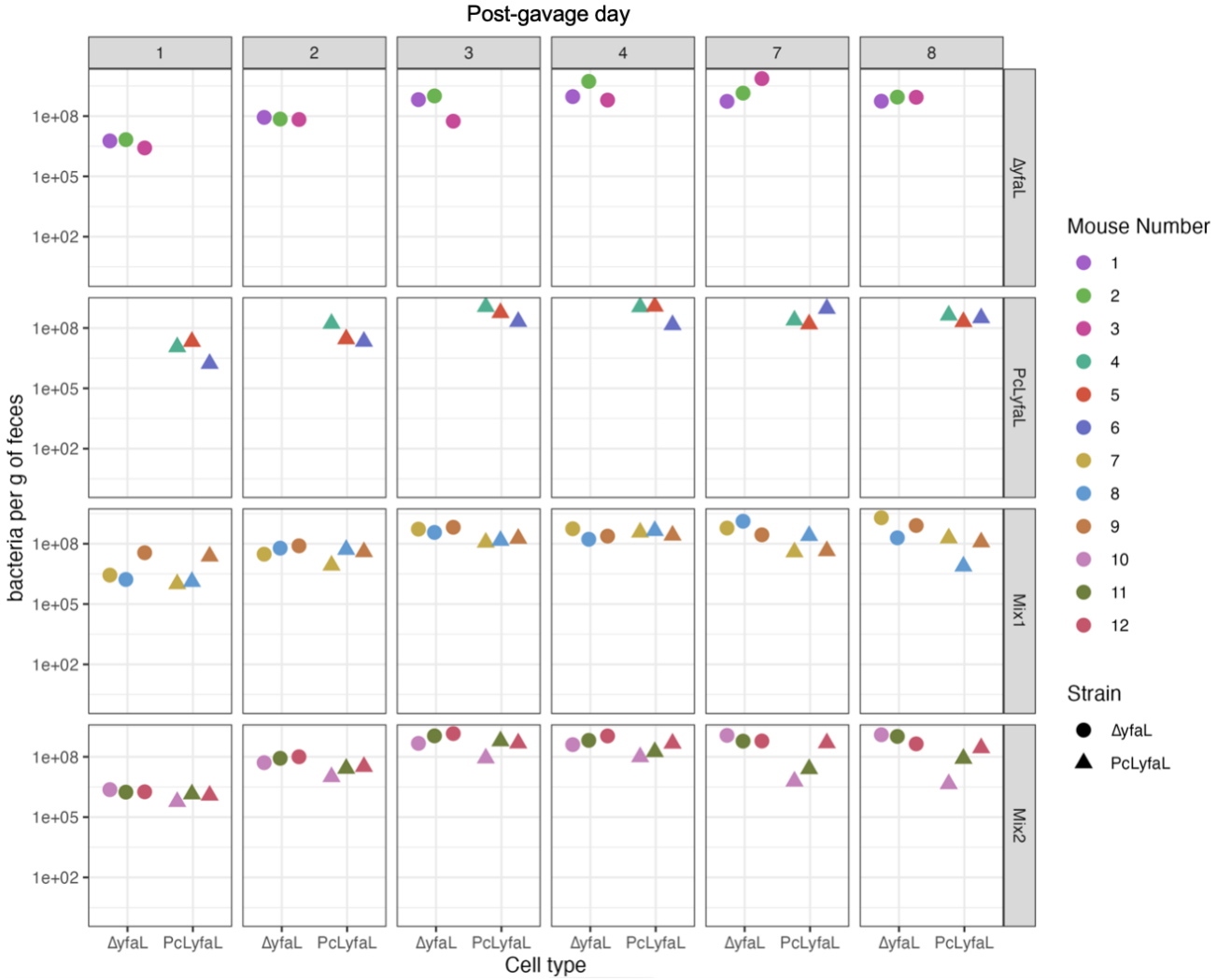

Supplementary Figure S7. **YfaL-mediated auto-aggregation does not improve GI tract colonization during competition experiments in mice.** Representation of the number of bacteria per g of feces found in mice colonized by WTΔ*yfaL* alone (first horizontal panel), PcL*yfaL* alone (second horizontal panel), or twice a 1:1 mix of WTΔ*yfaL* and PcL*yfaL* (mix1 and mix2, third and fourth horizontal panels). Each horizontal panel represent a cage containing 3 mice. Each vertical panel represent the day post inoculation. None of the comparison were found to be significative using a Kruskal-Wallis analysis of variance test ($p > 0.05$).

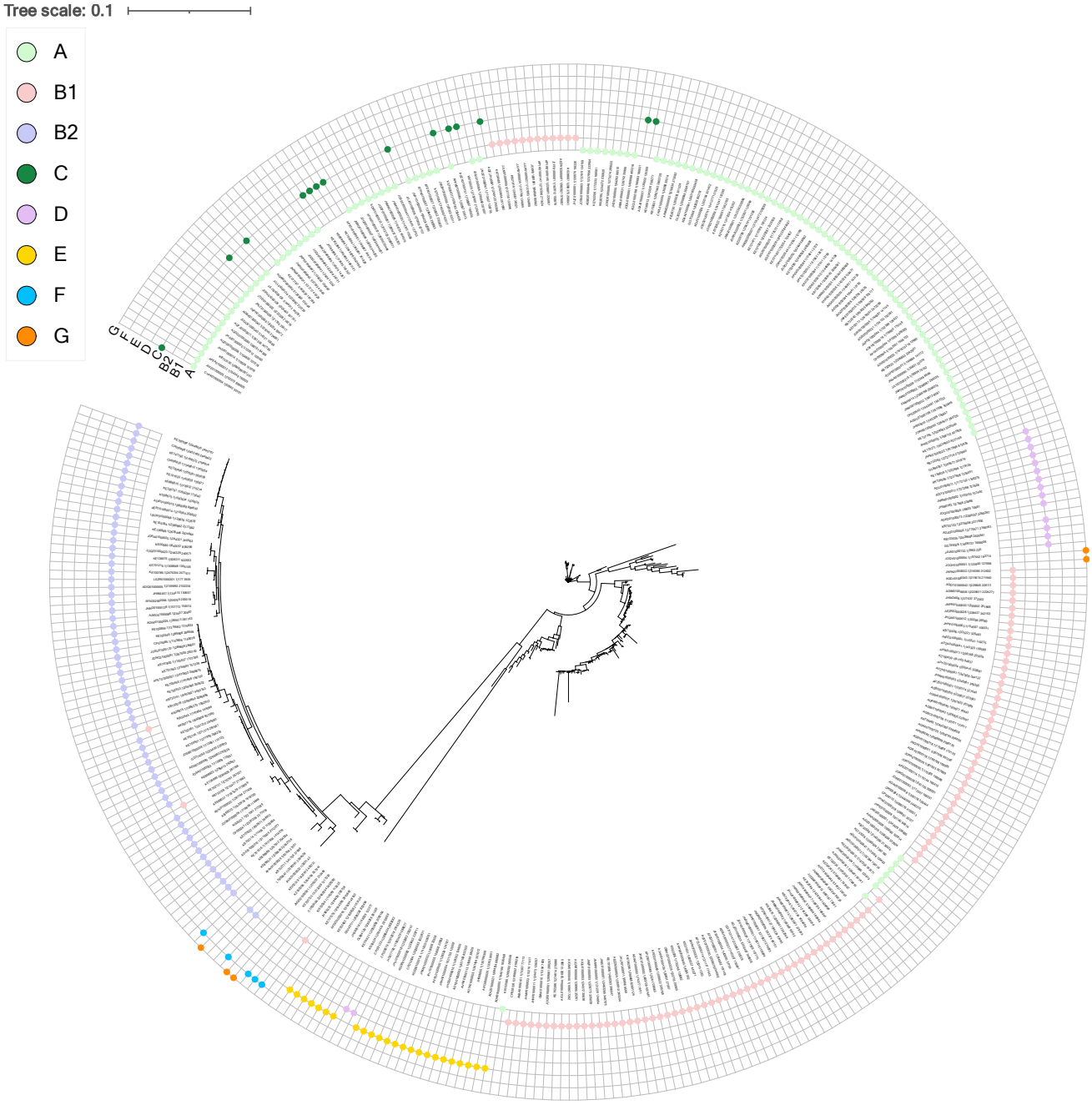

Supplementary Figure S8. Phylogenetic tree of 1819 YfaL protein sequences identified in 2053 *E. coli* genomes. The purple circles on the branches represent bootstrap values > 0.8. The different strain's phylogroups are displayed outside of the tree and each leaf label corresponds to the contig accession number on which the gene was identified followed by the corresponding coordinates as follows: contigID|start stop.

A high-resolution version of Supplementary Figure S8 is available at https://zenodo.org/records/13284193.

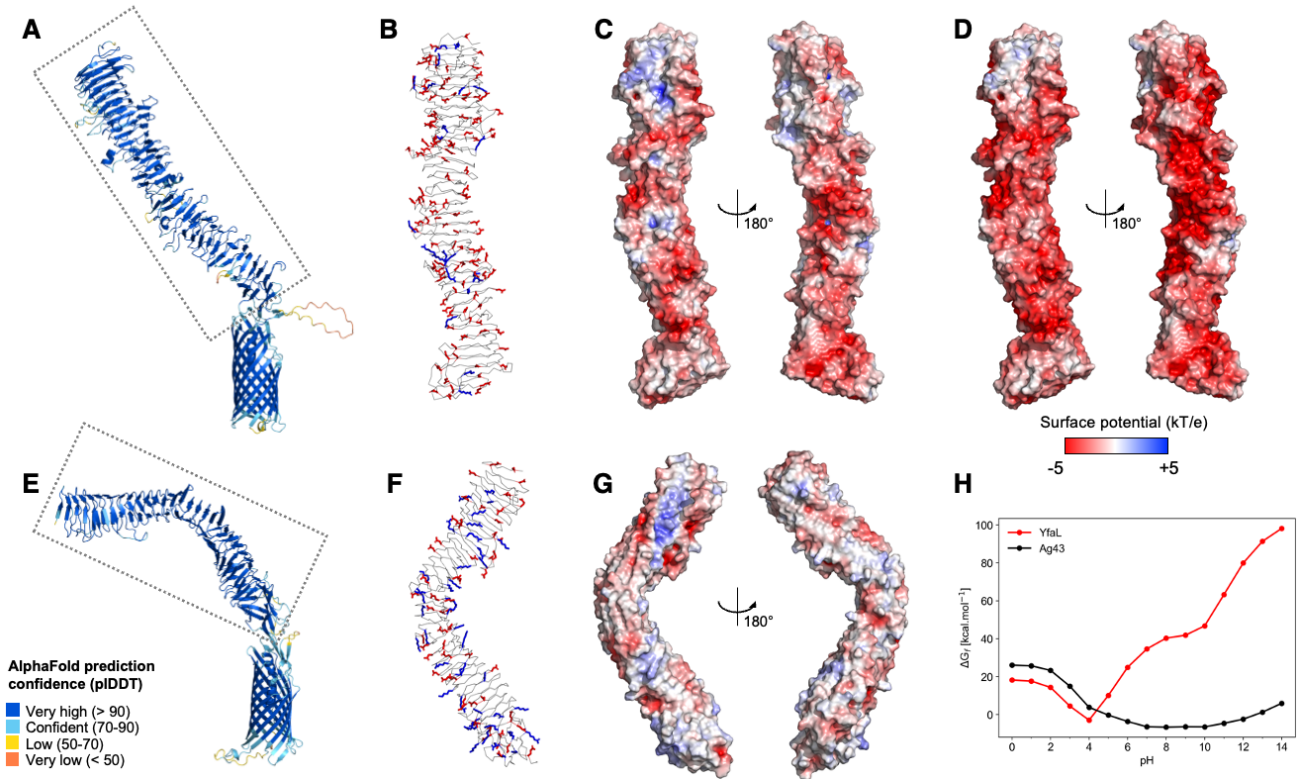

Supplementary Figure S9: Surface electrostatic profile for the YfaL and Ag43 passenger domains at different pH.

(A). AlphaFold (AF) model of full-length YfaL colored by predicted local distance difference test (pLDDT) values. The passenger domain is highlighted in the dashed box. (B). Passenger domain (residues 1 to 886) of YfaL AF model, where the side chains of acidic (Asp and Glu) and basic (Lys and Arg) residues are shown and colored in red and blue, respectively. (C). Electrostatic surface potential of YfaL passenger domain at pH 4.5 colored from red (negative) to blue (positive) as calculated with APBS and PDB2PQR. At pH 4.5, the total charge predicted by the AF model is -53. (D). Electrostatic surface potential of YfaL passenger domain at pH 7 colored from red (negative) to blue (positive) as calculated with APBS and PDB2PQR. At pH 7, the total charge predicted by the AF model is -87. (E). AF model of full-length Ag43 colored by predicted local distance difference test (pLDDT) values. The passenger domain is highlighted in the dashed box. (F). Passenger domain (residues 1 to 654) of Ag43 AF model, where the side chains of acidic (Asp and Glu) and basic (Lys and Arg) residues are shown and colored in red and blue, respectively. (G). Electrostatic surface potential of Ag43 passenger domain at pH 7 colored from red (negative) to blue (positive) as calculated with APBS and PDB2PQR. At pH 7, the total charge predicted by the AF model is -14. (H). Predicted profile for the free energy of folding according to the pH for the YfaL (red) and Ag43 (black) passenger domains as calculated with PROPKA.

SUPPLEMENTARY TABLES

Strain	Description	Source
E. coli MG1655	F^-,λ^-, *rph-1*	*E. coli* genetic stock center CGSC#6300.
MG1655 Δ*ag43*::Cm (**WT in this study**)	Deletion of a*g43,* CmR	[9]
MG1655 Δ*ag43*::Km	Deletion of a*g43*, KmR	[8]
MG1655 Δ*ag43*::Cm, Δ*yfaL*::FRT	Deletion of *ag43*, deletion of *yfaL*, CmR	This study
MG1655 pBAD*ag43*, CFP	*ag43* placed under control of the pBAD promoter, CFP::Amp at □ATT site, AmpR, CmR	This study
MG1655 pBAD*ag43*, YFP	*ag43* placed under control of the pBAD promoter, YFP::Amp at □ATT site, AmpR, CmR	This study
MG1655 Δ*ag43* pBAD*ypjA*, CFP	Deletion of *ag43*::Km, *ypjA* placed under control of the pBAD promoter, CFP::Amp at □ATT site, AmpR, CmR, KmR	This study
MG1655 Δ*ag43* pBAD*ypjA*, YFP	Deletion of *ag43*::Km, *ypjA* placed under control of the pBAD promoter, YFP::Amp at □ATT site, AmpR, CmR, KmR	This study
MG1655 Δ*ag43* pBAD*yeeJ*, CFP	Deletion of *ag43*::Km, *yeeJ* placed under control of the pBAD promoter, CFP::Amp at □ATT site, AmpR, CmR, KmR	This study
MG1655 Δ*ag43* pBAD*yeeJ*, YFP	Deletion of *ag43*::Km, *yeeJ* placed under control of the pBAD promoter, YFP::Amp at □ATT site, AmpR, CmR, KmR	This study
MG1655 Δ*ag43* pBAD*ycgH*, CFP	Deletion of *ag43*::Km, *ycgH* placed under control of the pBAD promoter, CFP::Amp at □ATT site, AmpR, CmR, KmR	This study
MG1655 Δ*ag43* pBAD*ycgH*, YFP	Deletion of *ag43*::Km, *ycgH* placed under control of the pBAD promoter, YFP::Amp at lambda ATT site, AmpR, CmR, KmR	This study
MG1655 Δ*ag43* pBAD*ydhQ*, CFP	Deletion of *ag43*::Km, *ydhQ* placed under control of the pBAD promoter, CFP::Amp at lambda ATT site, AmpR,	This study

	CmR, KmR	
MG1655 Δ*ag43* pBAD*ydhQ*, YFP	Deletion of *ag43*::Km, *ydhQ* placed under control of the pBAD promoter, YFP::Amp at lambda ATT site, AmpR, CmR, KmR	This study
MG1655 Δ*ag43* pBAD*ycgV*, CFP	Deletion of *ag43*::Km, *ycgV* placed under control of the pBAD promoter, CFP::Amp at lambda ATT site, AmpR, CmR, KmR	This study
MG1655 Δ*ag43* pBAD*ycgV*, YFP	Deletion of *ag43*::Km, *ycgV* placed under control of the pBAD promoter, YFP::Amp at lambda ATT site, AmpR, CmR, KmR	This study
MG1655 Δ*ag43* pBAD*yfaL*, CFP	Deletion of *ag43*::Km, *ypjA* placed under control of the pBAD promoter, CFP::Amp at lambda ATT site, AmpR, CmR, KmR	This study
MG1655 Δ*ag43* pBAD*yfaL*, YFP	Deletion of *ag43*::Km, *ypjA* placed under control of the pBAD promoter, YFP::Amp at lambda ATT site, AmpR, CmR, KmR	This study
MG1655 Δ*ag43* KmPcL*fim*, CFP	Deletion of *ag43*::Cm, *fim* placed under control of the PcL promoter, CFP::Amp at lambda ATT site, AmpR, KmR, CmR	This study
MG1655 Δ*ag43* KmPcL*fim*, YFP	Deletion of *ag43*::Cm, *fim* placed under control of the PcL promoter, YFP::Amp at lambda ATT site, AmpR, KmR, CmR	This study
MG1655 Δ*ag43* KmPcL*yad*, CFP	Deletion of *ag43*::Cm, *yad* placed under control of the PcL promoter, CFP::Amp at lambda ATT site, AmpR, KmR, CmR	This study
MG1655 Δ*ag43* KmPcL*yad*, YFP	Deletion of *ag43*::Cm, *yad* placed under control of the PcL promoter, YFP::Amp at lambda ATT site, AmpR, KmR, CmR	This study
MG1655 Δ*ag43* KmPcL*ycb*, CFP	Deletion of *ag43*::Cm, *ycb* placed under control of the PcL promoter, CFP::Amp at lambda ATT site, AmpR, KmR, CmR	This study
MG1655 Δ*ag43* KmPcL*ycb*, YFP	Deletion of *ag43*::Cm, *ycb* placed under control of the PcL promoter, YFP::Amp at	This study

	lambda ATT site, AmpR, KmR, CmR	
MG1655 Δ*ag43* KmPcL*yfc*, CFP	Deletion of *ag43*::Cm, *yfc* placed under control of the PcL promoter, CFP::Amp at lambda ATT site, AmpR, KmR, CmR	This study
MG1655 Δ*ag43* KmPcL*yfc*, YFP	Deletion of *ag43*::Cm, *yfc* placed under control of the PcL promoter, YFP::Amp at lambda ATT site, AmpR, KmR, CmR	This study
MG1655 Δ*ag43* KmPcL*yeh*, CFP	Deletion of *ag43*::Cm, *yeh* placed under control of the PcL promoter, CFP::Amp at lambda ATT site, AmpR, KmR, CmR	This study
MG1655 Δ*ag43* KmPcL*yeh*, YFP	Deletion of *ag43*::Cm, *yeh* placed under control of the PcL promoter, YFP::Amp at lambda ATT site, AmpR, KmR, CmR	This study
MG1655 Δ*ag43* KmPcL*sfm*, CFP	Deletion of *ag43*::Cm, *sfm* placed under control of the PcL promoter, CFP::Amp at lambda ATT site, AmpR, KmR, CmR	This study
MG1655 Δ*ag43* KmPcL*sfm*, YFP	Deletion of *ag43*::Cm, *sfm* placed under control of the PcL promoter, YFP::Amp at lambda ATT site, AmpR, KmR, CmR	This study
MG1655 Δ*ag43* KmPcL*yra*, CFP	Deletion of *ag43*::Cm, *yra* placed under control of the PcL promoter, CFP::Amp at lambda ATT site, AmpR, KmR, CmR	This study
MG1655 Δ*ag43* KmPcL*yra*, YFP	Deletion of *ag43*::Cm, *yra* placed under control of the PcL promoter, YFP::Amp at lambda ATT site, AmpR, KmR, CmR	This study
MG1655 Δ*ag43* KmPcL*ybg*, CFP	Deletion of *ag43*::Cm, *ybg* placed under control of the PcL promoter, CFP::Amp at lambda ATT site, AmpR, KmR, CmR	This study
MG1655 Δ*ag43* KmPcL*ybg*, YFP	Deletion of *ag43*::Cm, *ybg* placed under control of the PcL promoter, YFP::Amp at lambda ATT site, AmpR, KmR, CmR	This study
MG1655 Δ*ag43* KmPcL*yfaL* (**PcL*yfaL* in this study**)	Deletion of *ag43*::Cm, *yfaL* placed under control of the	This study

	PcL promoter, CmR, KmR	
MG1655 Δ*ag43* Δ*yfaL* λATT::KmPcL*yfaL*	Deletion of *ag43*::Cm, *yfaL* deleted from its original locus and placed under control of the PcL promoter at the lambda ATT site, CmR, KmR	This study
MG1655 Km*PcL*yfaL, Δ*ag43,* Δ*fimAH*, Δ*fliER,* Δ*csgA*	Deletion of *ag43,* deletion of *fim* operon, deletion of *fliE-R* operon, deletion of *csgA*, *yfaL* under control of the PcL promoter, CmR, KmR, ZeoR, SpecR	This study
MG1655 StrepR Δ*ag43*::Km Mars	Resistant to streptomycin, deletion of *ag43,* Mars::Zeo at lambda ATT site, StrepR, KmR, ZeoR	This study
MG1655 StrepR Δ*ag43*::Km CmPcL*yfaL* GFP	Resistant to streptomycin, deletion of *ag43, yfaL* placed under control of the PcL promoter, GFP::Zeo at lambda ATT site, StrepR, KmR, ZeoR, CmR	This study
Plasmid	**Description**	**Source**
pKOBEGA	pSC101 thermosensitive (replicates at 30°C), *araC*, arabinose-inducible λredγβα operon, AmpR	[10]
pCP20	Thermosensitive, encode yeast recombinase gene *flp* (flippase), AmpR	[11]

Supplementary Table S1. Strains and plasmids used in this study.

Name	Sequence 5'-> 3'
YfaL_500-3	tgcaggaaaccgtggaagagcacgc
KmFRT.verif3	cagtcatagccgaatagcct
KmFRT.verif5	ggattcatcgactgtggccg
yfaL-500-5	aggtcagacaaggtgtccgg
Ag43-ext-5	atacgctggtcagtgcgctc
Ag43-ext-3	atcagtgacggtgaaatatc
λATT-ext5	ggcgataaattgccgcatcg
λATT-ext3	tgccaccatcaagggaaagccc
L5-yfaL-labmda.ATT	ctttttgtctttttaccttcccgtttcgctcaagttagtaattctcaccaataaaaaacgcccgg
L3-yfaL-lambda.ATT	atgaaatagaaaaatgaatccgttgaagcctgctttttttattaccatttcaccgtcatcgacaaa
CmPcLyfaL_L5	gaaagatattccatatcgtataatgcgattaaatacgccgattctcaccaataaaaaacg
CmPcLyfaL_L3	gataatccgcatattaatctaaccatcattttctataagatagtacatgcaaccattatc
YfaL ATG +100_3	ctcgctttgacatcatatccctggc
cat-verif-3	gtacattgagcaactgactg
cat-verif-5	tacgcaaggcgacaaggtgc
qPCR yfaL 2 .Rev	ttcaatcaccacaccacgcc
qPCR yfaL 2.for	gcacggtaatcagaagcaaggg

Supplementary Table S2. Primers used in this study.

Strains	Adhesion forces (nN)	Rupture distances (nm)
WT (n=946)	0.270 ± 0.175	270 ± 119
+ fruc (n=955)	0.282 ± 0.177	296 ± 107
PcL*yfaL* (n=1384)	0.294 ± 0.181	338 ± 154
+ fruc (n=1005)	0.466 ± 0.195	421 ± 157

Supplementary Table S3. Averaged values of hydrophobic adhesion force and rupture distance measured on *E. coli* WT and *E. coli* PcL*yfaL* strains grown in LB with or without 0.3% fructose. The hydrophobic adhesion force and the rupture distance were evaluated from the analysis of the *last* rupture event of the cell-to-tip retraction force curve. Each value indicated in the table corresponds the average over n (specified) distinct retraction curves collected at different positions (pixels) of the probed cell surface. These data were obtained from experiments performed on 10 individual bacterial cells at least.

pH 4.6 (data in **Figure 4A,B**)			**pH 5.7** (data in **Supplementary Fig. S9**)		
	ρ_o/F (mM)	$1/\lambda_o$ (nm)		ρ_o/F (mM)	$1/\lambda_o$ (nm)
WT without fructose	-64	1.1	WT without fructose	-88	1.1
WT with 0.2% fructose	-76	1	WT with 0.3% fructose	-118	0.8
PcL*yfaL* without fructose	-50	1.3	PcL*yfaL* without fructose	-71	1.2
PcL*yfaL* with 0.3% fructose	-6	5.4	PcL*yfaL* with 0.2% fructose	-37	2.3

Supplementary Table S4. Summary of the electrohydrodynamic parameters ρ_o (charge density pertaining to the electrokinetically active cell surface layer) and $1/\lambda_o$ (electroosmotic flow penetration length within this cell surface layer) derived from the fitting of the electrophoretic data given in **Figure 4** and **Supplementary Fig. S9** using soft surface electrophoresis (SSE) theory (cf. details in the Methods section, and Eqs. (1)-(4) therein). The charge density is here reported in the form of the equivalent concentration ρ_o/F (including sign) of elementary charges, where F is the Faraday number. All theoretical parameters are obtained with ca. 10% error as estimated from the standard deviations of the measured electrophoresis data.

Supplementary Table S5. Analysis of autotransporter prevalence. This table can be downloaded at https://zenodo.org/records/12724448.

Table S5A- Table showing the presence / absence of all 13 AIDA-I ATs in each of the 2053 genomes investigated. The phylogroup and strain name are shown in first two columns, respectively. **Table S5B**- Table showing the prevalence of each AIDA-I ATs among the 2053 genomes investigated. In the first column, each AT name is followed by the related Uniprot identifier

corresponding to K12 MG1655 sequence used for the identification. **Table S5C**- Table showing the numbers and proportions of strains in each phylogroup having in their genome each AIDA-I ATs.

Supplementary Table S6. YfaL sequence analysis. This table can be downloaded at https://zenodo.org/records/12725303.
Table S6A- Table showing parameters related to each YfaL sequence identified. The contig identifier and position of the sequence in it (column A), the strain name (column B), the phylogroup (column C), the size of each structural part of the sequence (column D to H), the number of mutations in these parts (column I to M), the related mutation frequency (column N to R). **Table S6B**- Table showing the number of YfaL sequences in each phylogroup as well as the related mutation frequences in the whole sequence and for each structural part of it.

Supplementary Table S7. *E. coli*'s genomes used in this study.
This table can be downloaded at https://zenodo.org/records/12725345.

Supplementary References

1. F. Quiles, A. Burneau and N. Gross, *Appl. Spectrosc.*, 1999, **53**, 1061-1070.
2. D. P. Clark, *FEMS Microbiol Rev*, 1989, **5**, 223-234.
3. M. Carbonaro and A. Nucara, *Amino Acids*, 2010, **38**, 679-690.
4. C. H. Posten and C. L. Cooney, in *Biotechnology, A Comprehensive Treatise, Volumes 1 - 8*, ed. D. G. R. Prof. Dr. H.-J. Rehm, Wiley, 2001, vol. 1, ch. 3, pp. 111-162.
5. F. Quilès, F. Humbert and A. Delille, *Spectrochim Acta A Mol Biomol Spectrosc*, 2010, **75**, 610-616.
6. J. F. L. Duval and H. Ohshima, *Langmuir*, 2006, **22**, 3533-3546.
7. F. Gaboriaud, E. Dague, S. Bailet, F. Jorand, J. F. L. Duval and F. Thomas, *Colloids Surf B Biointerfaces*, 2006, **52**, 108-116.
8. G. Francius, P. Polyakov, J. Merlin, Y. Abe, J. M. Ghigo, C. Merlin, C. Beloin and J. F. L. Duval, *PLoS One*, 2011, **6**, e20066.
9. A. Roux, C. Beloin and J. M. Ghigo, *Journal of bacteriology*, 2005, **187**, 1001-1013.
10. M.-K. Chaveroche, J.-M. Ghigo and C. d'Enfert, *Nucleic acids research*, 2000, **28**, e97-e97.
11. P. P. Cherepanov and W. Wackernagel, *Gene*, 1995, **158**, 9-14.